Ceramics International xxx (xxxx) xxx–xxx

Contents lists available at ScienceDirect

Ceramics International

journal homepage: www.elsevier.com/locate/ceramint

High relative permittivity $Bi_4B_{2+x}O_{9+3x/2}$ (x = 1.5, 2, 2.5, 3) microwave ceramics for ULTCC technology

Kangguo Wang, Huanfu Zhou*, Xianjie Zhou, Xiaowen Luan, Sang Hu, Jiji Deng, Shixuan Li, Xiaobin Liu

Collaborative Innovation Centre for Exploration of Hidden Nonferrous Metal Deposits and Development of New Materials in Guangxi, Key Laboratory of Nonferrous Materials and New Processing Technology, Ministry of Education, School of Materials Science and Engineering, Guilin University of Technology, Guilin, 541004, China

ARTICLE INFO

Keywords:
$Bi_4B_{2+x}O_{9+3x/2}$ ceramics
High relative permittivity
ULTCC
Microwave dielectric properties

ABSTRACT

$Bi_4B_{2+x}O_{9+3x/2}$ (x = 1.5, 2, 2.5, 3) compounds with high relative permittivity and ultra-low sintering temperature were prepared using the conventional solid-state method. Due to the volatilisation of B_2O_3 during sintering, a $Bi_4B_2O_9$ single phase was obtained in excess addition of boric acid for x = 2.5. The densest structure of the $Bi_4B_{2+x}O_{9+3x/2}$ (x = 2.5) ceramic, sintered at 585 °C, exhibited good microwave dielectric properties of a relative permittivity (ε_r) = 42.5, quality factor ($Q \times f$) = 3240 GHz, and temperature coefficient of resonance frequency (τ_f) = −59 ppm/°C. As the value of x changed, the second phases of Bi_2O_3 and $Bi_3B_5O_{12}$ appeared, and the (ε_r) and (τ_f) values decreased. The $Bi_4B_{2+x}O_{9+3x/2}$ (x = 2.5) ceramics did not react with either Ag or Al, indicating that they are good candidate materials for ultra-low temperature co-fired ceramic (ULTCC) applications.

1. Introduction

As 5G technology becomes part of daily life, people's demand for communication equipment is continuously increasing. Different from low-temperature cofired ceramic (LTCC) technology, ultra-LTCC (ULTCC) technology requires a lower sintering temperature and the ceramic materials to be densified at temperatures below 700 °C, and they do not react with Al or other low melting point materials to ensure co-firing [1–7].

ULTCC technology provides the possibility for microwave dielectric ceramics to be used in small portable equipment. However, relative permittivity will limit the application of microwave dielectric ceramics in devices of different sizes [8,9]. The wavelength of an electromagnetic wave (λ) can be calculated using Equation (1):

$$\lambda = \lambda_0 / \sqrt{\varepsilon_r}, \quad (1)$$

where λ_0 is the wavelength in a vacuum and ε_r is the relative permittivity of a microwave ceramic. At the same resonant frequency f_0, the larger the ε_r of the dielectrics, the smaller the wavelength, and the smaller the size of the corresponding dielectric resonator; hence, more electromagnetic energy can be concentrated in the medium [10]. In other words, a high permittivity is beneficial to the miniaturization and high quality of dielectric resonators. However, only a few studies on microwave dielectric ceramics focus on both an ultra-low sintering temperature and high dielectric constant.

Currently, studies on ULTCC are scarcer than other literature on microwave dielectric ceramics, as shown in Fig. 1. In addition, the majority of the relevant studies focus on low relative permittivity systems because a lower relative permittivity of a microwave ceramic translates to lower microwave dielectric loss [11,12]. Only $(Li_{0.5}Bi_{0.5})MoO_4$ ceramic was studied with high relative permittivity greater than 40 and low sintering temperature lower than 700 °C; its ceramic sintered at 560 °C exhibited good microwave dielectric properties of ε_r = 44.4, quality factor ($Q \times f$) = 3200 GHz, and temperature coefficient of the resonance frequency (τ_f) = +245 ppm/°C [13,14]. Microwave dielectric properties of ε_r = 39, $Q \times f$ = 2600 GHz, and τ_f = −203 ppm/°C for $Bi_4B_2O_9$ sintered at 660 °C were reported by Chen et al. [15]. However, the harsh preparation process (using isopropanol as the ball milling medium), high negative temperature coefficient of resonance frequency, and lack of tests of co-firing with Al limits its further development.

In our previous research [16], $Bi_3B_{5+x}O_{12+3x/2}$ (x = 0–6) compounds for x = 4 exhibited a $Bi_3B_5O_{12}$ single phase, an ultra-low sintering temperature of 625 °C, and good microwave dielectric properties of ε_r = 12.14, $Q \times f$ = 14,800 GHz, and τ_f = −72 ppm/°C. Lowering the x value caused the appearance of the $Bi_4B_2O_9$ second phase, which

* Corresponding author.
E-mail address: zhouhuanfu@163.com (H. Zhou).

https://doi.org/10.1016/j.ceramint.2020.02.176
Received 7 January 2020; Received in revised form 13 February 2020; Accepted 17 February 2020

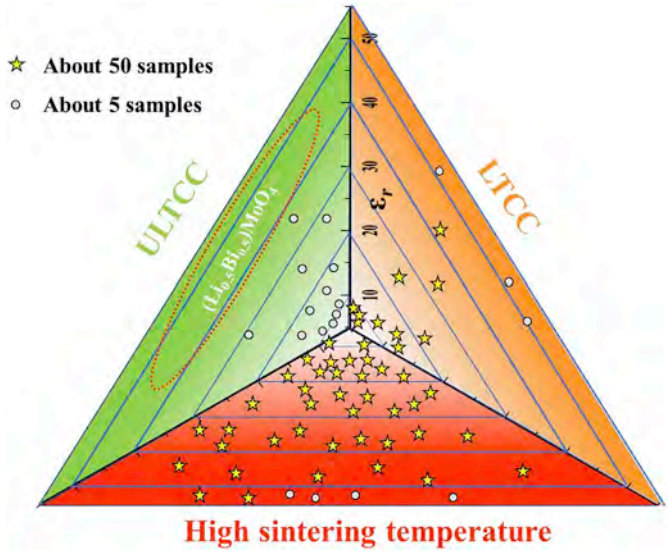

Fig. 1. Application of microwave dielectric ceramics with different relative permittivities at different sintering temperatures.

led to a decrease in the $Q \times f$ value and increase in the ε_r value from 12.14 to 18.81. In this study, the composites of $Bi_4B_{2+x}O_{9+3x/2}$ (x = 1.5, 2, 2.5, 3) were designed and prepared using H_3BO_3 and Bi_2O_3 powders, and their microwave dielectric properties, sintering behaviours, microstructures, and compatibilities with aluminium and silver were investigated.

2. Experimental procedure

$Bi_4B_{2+x}O_{9+3x/2}$ (x = 1.5, 2, 2.5, 3) ceramics were prepared using a conventional solid-state reaction method. High-purity raw powders of Bi_2O_3 (99.95%) and H_3BO_3 (99.99%) were stoichiometrically weighted, mixed, and ball-milled in alcohol using zirconia balls for 6 h and subsequently dried at 90 °C in a drying oven. Subsequently, the dry powders were calcined in air at 550 °C for 4 h. The fine calcined powders were granulated by using 5 wt% polyvinyl alcohol (PVA) and subsequently pressed into cylinders with a diameter of 10 mm and thickness of 4–6 mm under a pressure of approximately 200 MPa. Finally, the disks were heated in air to 500 °C for 4 h to exhaust the binder and subsequently sintered at 555–595 °C for 4 h at a heating rate of 5 °C/min.

The crystalline phases of the ceramics were determined using an X-ray diffractometer (XRD; Model X'Pert PRO, PANalytical, Almelo, Netherlands) at a scan rate of 0.417°/s and Cu Kα radiation generated at 40 kV and 40 mA. Rietveld refinement data were obtained at a low scan rate (0.021°/s) using GSAS software to further calculate the relative phase contents. Scanning electron microscopy (SEM; Model JSM6380-LV, JEOL, Tokyo, Japan) was used to observe the microstructures of the natural surfaces of the ceramics. In thermal etching, all cross sections of the samples were polished and heated at 50 °C below their sintering temperature for 30 min. The relative densities of the ceramics were calculated using Equation (2):

$$\rho_r = \rho_b / \rho_C, \tag{2}$$

where ρ_r, ρ_b, and ρ_C are the relative density, bulk density, and theoretical density of the ceramics, respectively. The bulk density was measured using Archimedes' method.

The dielectric behaviour in the microwave frequency range was tested using the TE01δ method via a network analyser (E5071C, Agilent Co., CA, USA, 10 MHz to 20 GHz). The τ_f values were calculated using Equation (3):

$$\tau_f = \frac{f_T - f_{T_0}}{f_{T_0}(T - T_0)} \tag{3}$$

where f_T and f_{T_0} are the resonant frequencies at 80 and 25 °C, respectively.

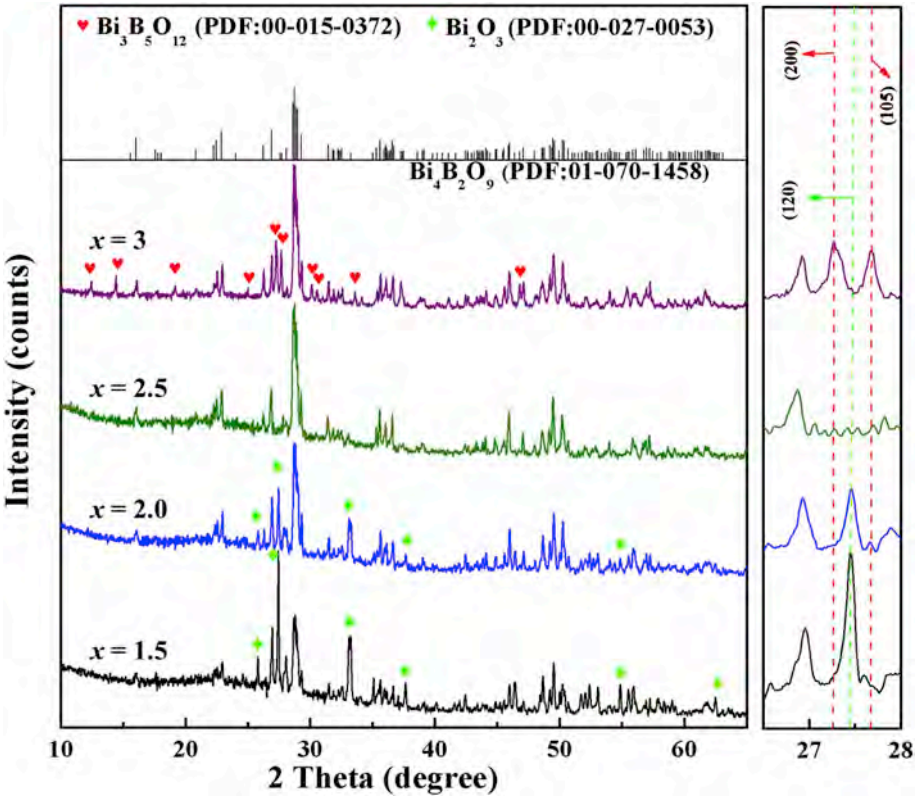

Fig. 2. The room-temperature XRD patterns of $Bi_4B_{2+x}O_{9+3x/2}$ (x = 1.5, 2, 2.5, 3) ceramics sintered at the optimum sintering temperature.

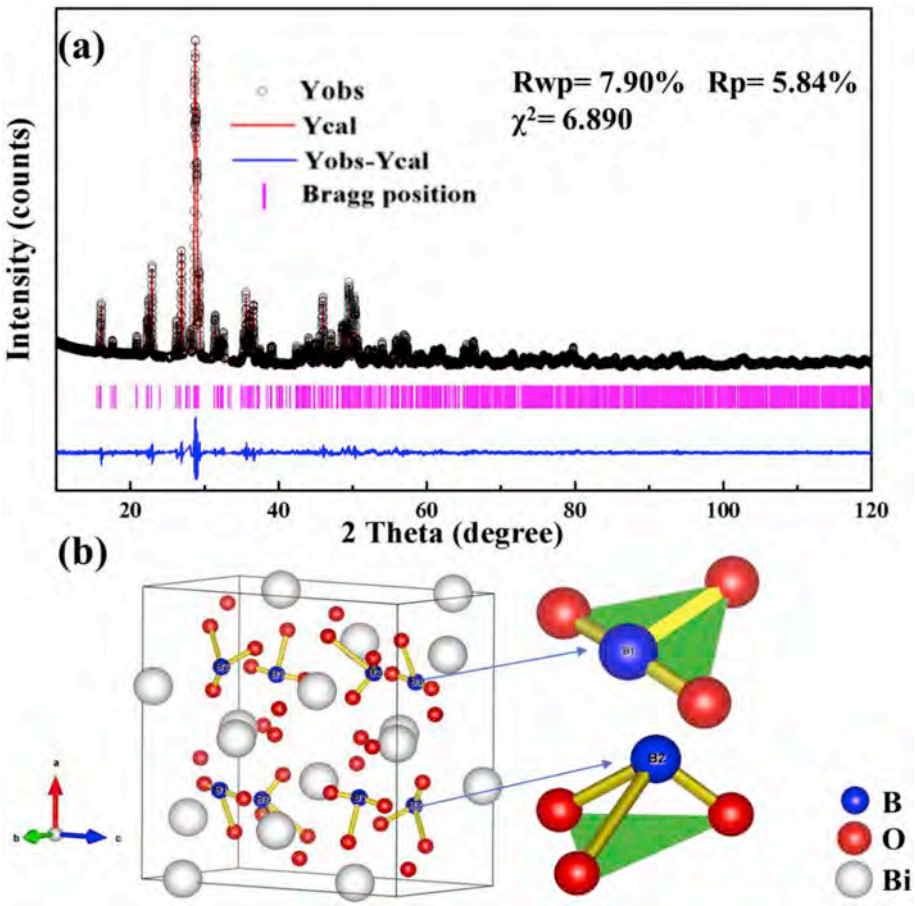

Fig. 3. (a) Rietveld refinement of the room-temperature XRD data of $Bi_4B_{2+x}O_{9+3x/2}$ (x = 2.5). (b) A crystal structure schematic for that ceramic.

3. Results and discussion

The room-temperature XRD patterns of $Bi_4B_{2+x}O_{9+3x/2}$ (x = 1.5, 2, 2.5, 3) ceramics sintered at their optimum temperatures are illustrated in Fig. 2. When x = 1.5 and 2, the pure phase structure of $Bi_4B_2O_9$ cannot be obtained; instead, $Bi_4B_2O_9$ and Bi_2O_3 phases are obtained because of the volatilisation of B_2O_3. As the value of x increased to 2.5, the extra Bi_2O_3 participated in the reaction because of the addition of excessive H_3BO_3, indicated by the disappearance of the peak on the (120) crystal plane, which caused only a single phase of monoclinic $Bi_4B_2O_9$ (PDF: 01-070-1458). As x further increased to 3, a $Bi_3B_5O_{12}$ (PDF: 01-015-0372) second phase with orthorhombic structure was observed in the XRD result, which was indicated by the appearance of (200) and (105) peaks.

The Rietveld refinement result for the $Bi_4B_{2+x}O_{9+3x/2}$ (x = 2.5) sample processed by the GSAS software is shown in Fig. 3 [17]. The R-values with Rwp = 7.90%, Rp = 5.83%, and χ^2 = 6.89 were obtained by using the crystal structure of $Bi_4B_2O_9$ (See ICSD: 2796) as the reference standard for refinement. These low R-values suggest that the XRD data test result of ceramic matched well with $Bi_4B_2O_9$ for the monoclinic structure in the space group P21/c. The refined cell parameters were a = 11.11589(8) Å, b = 63,444(5) Å, c = 11.04526(8) Å, $\alpha = \gamma = 90°$, β = 91.0198(7)°, and V = 814.434(10) Å^3. The atomic coordinates are listed in Table 1. Fig. 3(b) shows the structure cell of a $Bi_4B_{2+x}O_{9+3x/2}$ (x = 2.5) ceramic. There were two types of isolated $[BO_3]^{3-}$ trigonal coordinations—part triangle, part pyramidal—containing all boron of ceramic. This result was similar to the $Bi_4B_2O_9$ crystal structure in Egorysheva's study [18].

Fig. 4 depicts the micrographs of the free surfaces for $Bi_4B_{2+x}O_{9+3x/2}$ ceramics sintered at different temperatures. The porosity of $Bi_4B_{2+x}O_{9+3x/2}$ (x = 2.5) ceramics decreased as sintering temperature increased from 565 to 585 °C, as shown in Fig. 4(a) and (b). The ceramic exhibited a dense microstructure with distinct grain boundaries at 585 °C. As the sintering temperature further increased to 595 °C, a few pores appeared in the ceramic, as shown in Fig. 4(c). As Fig. 4(d) and (e) show, when x = 2 and 3, a dense morphology was obtained in the ceramics at 585 and 610 °C, respectively. However, the second phases of Bi_2O_3 and $Bi_3B_5O_{12}$ appeared. This result was consistent with the XRD analysis. The details of the results of the EDS analysis are shown in Fig. 5.

Fig. 6(a) illustrates the bulk and relative densities of $Bi_4B_{2+x}O_{9+3x/2}$ (x = 2.5) ceramic sintered at 555–595 °C. At the sintering

Table 1
Atomic coordinates of $Bi_3B_{5+x}O_{12+3x/2}$ (x = 4) and reliability factors.

Atom	Mult	x/a	y/b	z/c	Occ	Ui/Ue*100
Bi1	4e	0.992357	0.482339	0.346054	1	1.09
Bi2	4e	0.80679(21)	0.04379(28)	0.49051(19)	1	1.18
Bi3	4e	0.502179	0.424060	0.159545	1	0.98
Bi4	4e	0.342967	0.438888	0.481242	1	0.74
O1	4e	0.480223	0.095725	0.133001	1	1.24
O2	4e	0.4048(31)	0.1710(34)	0.5122(25)	1	1.66
O3	4e	0.8604(28)	0.2069(35)	0.3010(25)	1	0.21
O4	4e	0.9487(31)	0.1700(34)	0.0034(27)	1	2.11
O5	4e	0.1880(30)	0.2239(39)	0.1846(24)	1	1.53
O6	4e	0.6834(30)	0.2385(38)	0.3514(22)	1	1.14
O7	4e	0.1032(30)	0.2432(41)	0.3429(23)	1	1.97
O8	4e	0.3242(29)	0.2309(40)	0.2945(24)	1	2.30
O9	4e	0.6956(21)	0.2945(27)	0.1873(16)	1	−3.1(4)
B1	4e	0.691(4)	0.310(5)	0.2771(30)	1	−2.7(8)
B2	4e	0.215(6)	0.499(7)	0.1894(40)	1	−0.36

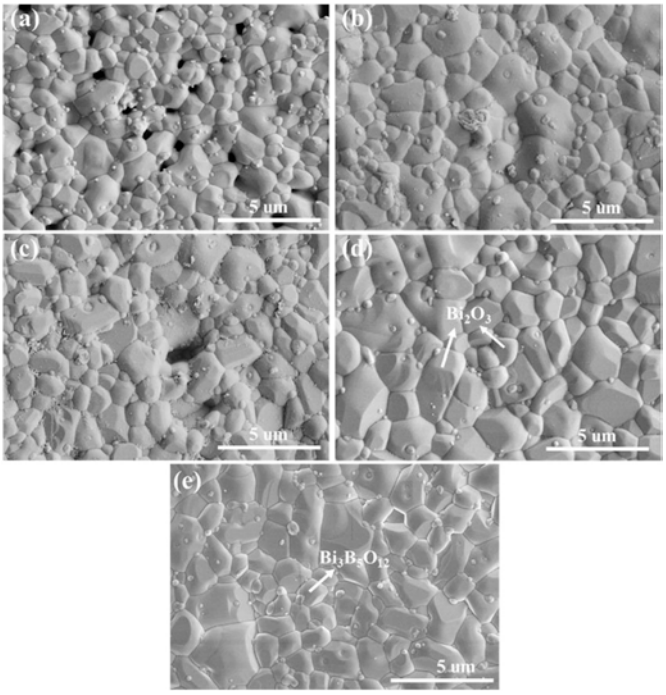

Fig. 4. SEM images of the $Bi_4B_{2+x}O_{9+3x/2}$ (x = 1.5, 2, 2.5, 3) ceramics sintered at different temperatures. [x = 2.5 sintered at 565 (a), 585 (b), and 595 °C (c); x = 2 sintered at 585 °C (d); x = 3 sintered at 610 °C (e)].

temperature of 585 °C, the bulk and relative density extended to the maximum values of 7.98 g/cm^3 and 97.54%, respectively. The SEM results (Fig. 4(a), (b), and (c)) indicated that the decrease in porosity and densification process completely caused the bulk and relative density of the ceramic to reach the peaks at 585 °C.

While the dielectric properties primarily depend on intrinsic factors such as ionic polarizability and lattice vibration, they also depend on extrinsic factors including density, phase composition, etc. [19,20]. The change trend in the relative permittivity of the $Bi_4B_{2+x}O_{9+3x/2}$ (x = 2.5) ceramics was the same as that in the relative density, as shown in Fig. 6. At the sintering temperature of 585 °C, the relative permittivity of ceramic attained the maximum value of 42.5 due to the most compact crystal structure. Bosman and Havinga's correction equation was applied to remove the influence of the porosity on the relative permittivity of the ceramics [21]:

$$\varepsilon_{co} = \varepsilon_m (1 + 1.5p) \quad (4)$$

where ε_{co}, ε_m, and p are the corrected and measured values of relative permittivity and porosity percentage, respectively. After the influence of pores was eliminated, the ε_{co} values of the $Bi_4B_{2+x}O_{9+3x/2}$ (x = 2.5) ceramic retained a relatively steady change along with the sintering temperature and were slightly higher than the measured values, as shown in Fig. 6(b). This result indicated that the change in porosity should be the most critical factor for the variation in the relative permittivity of ceramics. The theoretical relative permittivity (ε_{th}) can also be calculated using the Clausius-Mossotti equation [22]:

$$\varepsilon_{th} = \frac{3V + 8\pi\alpha}{3V - 4\pi\alpha} \quad (5)$$

where V is the molecular volume and α is the polarizability of the $Bi_4B_2O_9$ molecule. The total of ionic polarizability of $Bi_4B_2O_9$ can be predicted as follows:

$$\alpha(Bi_4B_2O_5) = 4\alpha(Bi^{3+}) + 2(B^{3+}) + 9(O^{2-}) \quad (6)$$

where $\alpha(Bi^{3+})$, $\alpha(B^{3+})$, and $\alpha(O^{2-})$ are the polarizability of

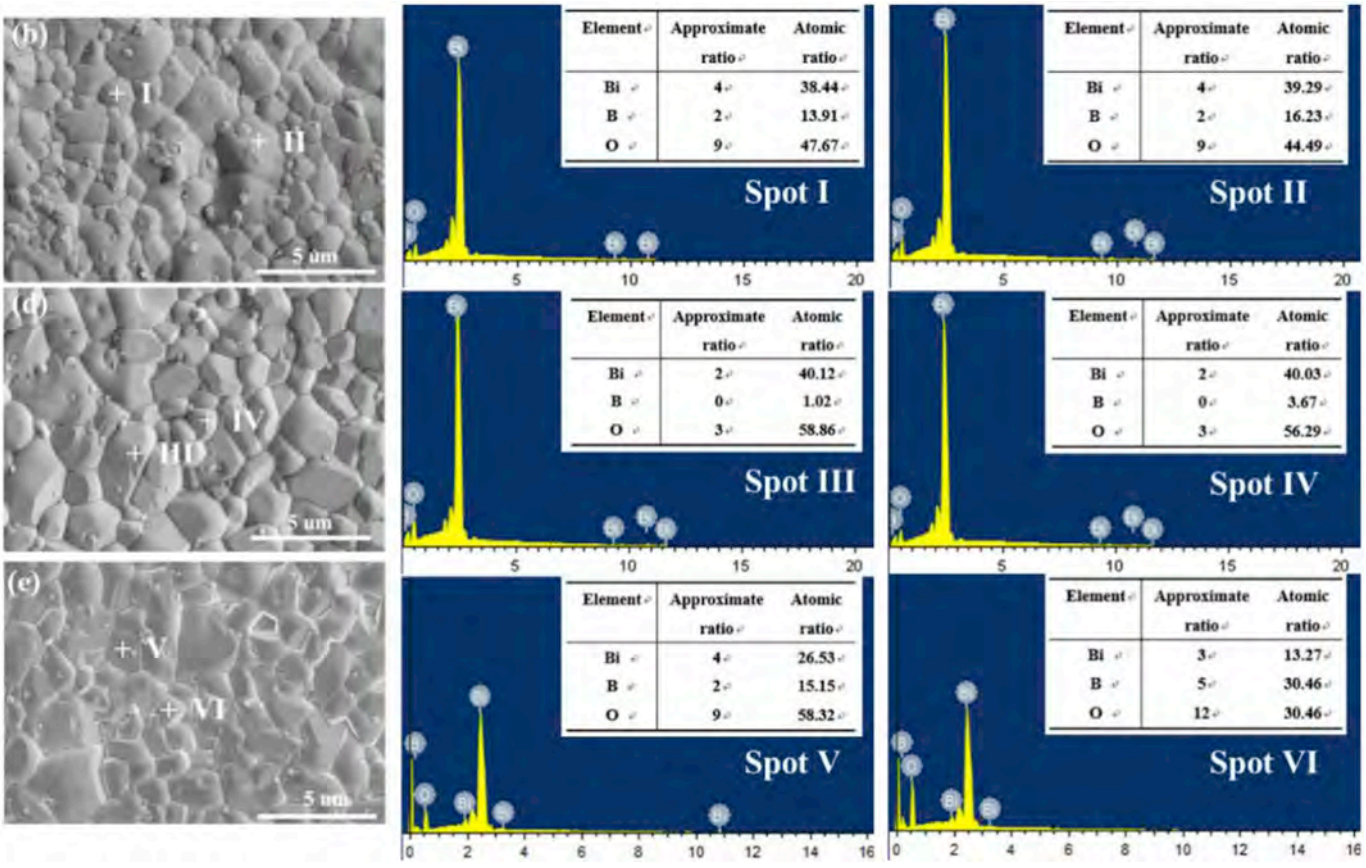

Fig. 5. EDS spectra of $Bi_4B_{2+x}O_{9+3x/2}$ (x = 2, 2.5, 3) ceramics at the optimum sintering temperature.

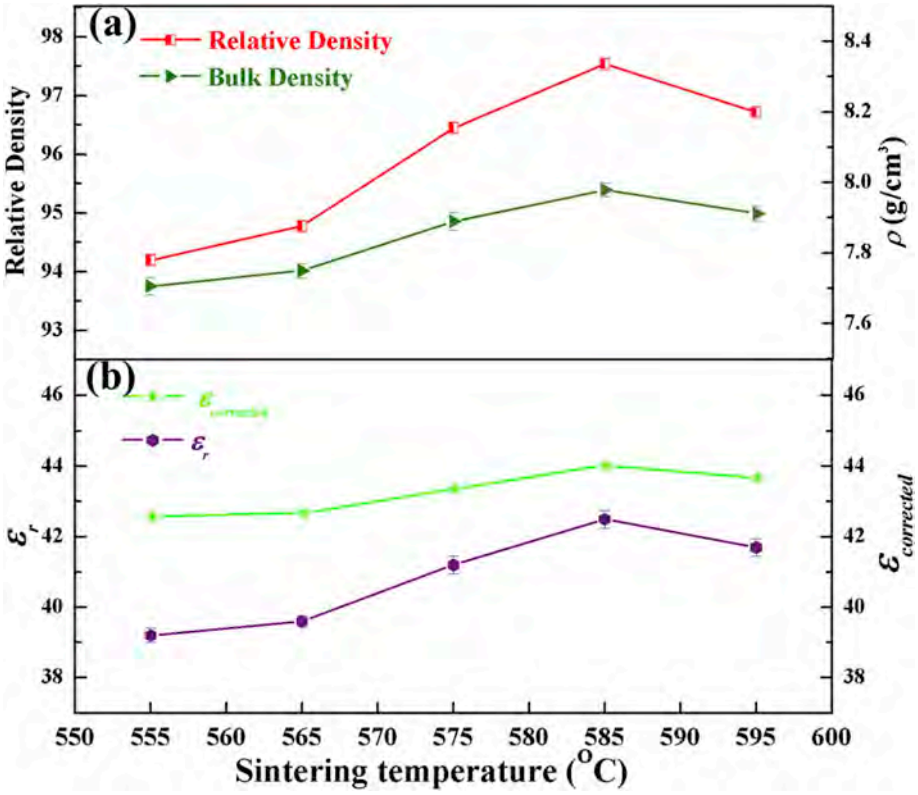

Fig. 6. The relative and bulk density (a), the relative permittivity and the corrected permittivity values (b) of the $Bi_4B_{2+x}O_{9+3x/2}$ (x = 2.5) ceramic as a function of sintering temperature.

Bi^{3+}(6.12 Å^3), B^{3+}(0.05 Å^3), and O^{2-} (2.01 Å^3). However, the ε_{th} of $Bi_4B_2O_9$ was approximately 22.56, which was much lower than the measured value (42.5). The inconsistency between ε_{th} and ε_r may have been caused by the participation of other polarization mechanisms in addition to ion polarization. A similar phenomenon also occurred in other systems [23,24].

Fig. 7 shows the trends of the $Q \times f$ and temperature coefficient of resonance frequency values for the $Bi_4B_{2+x}O_{9+3x/2}$ (x = 2.5) ceramic sintered at different temperatures. Similar to the change in relative permittivity, external and internal factors also affect the value of the microwave ceramic. Often, intrinsic losses depend on the lattice vibrations and phonon energy in crystals, and extrinsic losses to receive the secondary phases, morphology, porosity and so on many types of factors the influence [25,26]. At the best densification temperature of 585 °C, the $Bi_4B_{2+x}O_{9+3x/2}$ (x = 2.5) ceramic exhibited a maximum $Q \times f$ value of 3318 GHz at a low frequency of 5.39 GHz.

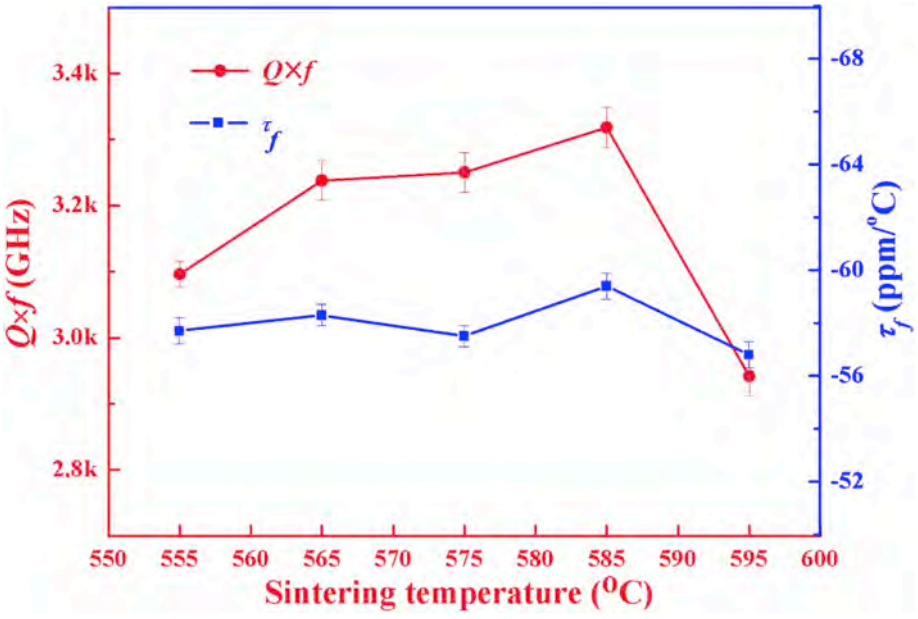

Fig. 7. The variation in the quality factor (a) and temperature coefficient of resonant frequency (b) of $Bi_4B_{2+x}O_{9+3x/2}$ (x = 2.5) ceramic as a function of sintering temperature.

Table 2
Densification temperatures, phase compositions, bulk densities, and microwave dielectric properties of $Bi_4B_{2+x}O_{9+3x/2}$ (x = 1.5, 2, 2.5, 3) ceramics.

x value	Ts (°C)	Phase compositions	$Q \times f$ (GHz)	ρ (g/cm^3)	ε_r	τ_f (ppm/°C)
1.5	585	$Bi_4B_2O_9$ and Bi_2O_3	3503	8.31	36.5	−132
2	585	$Bi_4B_2O_9$ and $Bi_{24}B_2O_{39}$	3381	8.29	39.5	−73
2.5	585	$Bi_4B_2O_9$	3240	7.79	42.5	−59
3	610	$Bi_4B_2O_9$ and $Bi_3B_5O_{12}$	4960	6.95	31.0	−76

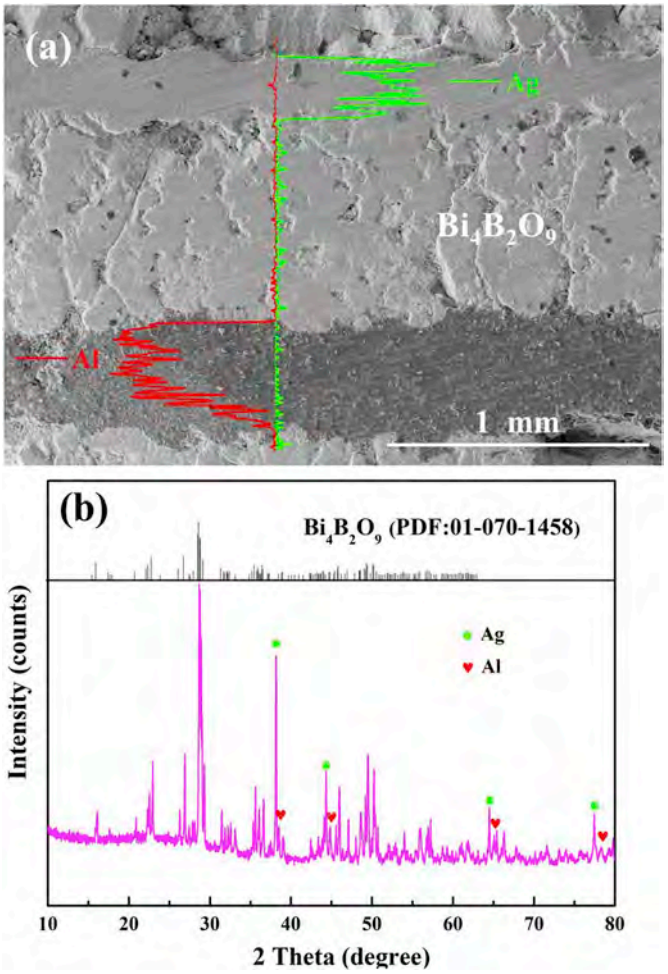

Fig. 8. SEM image of the $Bi_4B_{2+x}O_{9+3x/2}$ (x = 2.5) ceramic co-fired with Al and Ag powders (a); XRD patterns of the $Bi_4B_{2+x}O_{9+3x/2}$ (x = 2.5) ceramic with 25 wt% Al and 25 wt% Ag powder (b).

τ_f is well known to be closely related to the bond energy and bond length of a crystal, which is influenced by the preferred orientation of grains and phase transformation. However, the contribution of the porous rate to the τ_f of a ceramic is minimal. Hence, τ_f values of the $Bi_4B_{2+x}O_{9+3x/2}$ (x = 2.5) ceramic maintained a stable value between −56.8 and −59.4 ppm/°C as the sintering temperature changed because of the invariant phase composition. Note that this value was much higher than that of the pure $Bi_4B_2O_9$ ceramic reported by Chen [15].

The densification temperature, phase compositions, bulk density, and microwave dielectric properties of $Bi_4B_{2+x}O_{9+3x/2}$ (x = 1.5–3) ceramics are listed in Table 2. Pure Bi_2O_3 could be densified at approximately 680 °C with microwave dielectric properties of ε_r = 33, $Q \times f$ = 18,700 GHz, and τ_f = −235 ppm/°C. When the value of x was at a low level, due to the influence of the Bi_2O_3 second phase, the τ_f value of $Bi_4B_{2+x}O_{9+3x/2}$ ceramic maintained a large negative value of −132 ppm/°C. When x = 4, the ceramic exhibited high ε_r and small τ_f values of 42.5 and −59 °C, respectively, due to the $Bi_4B_2O_9$ single phase.

This can be explained by the mixing rule in the following equation [27]:

$$\tau_f = \sum_i^n v_i \tau_{fi} \quad (7)$$

where v_i and τ_{fi} are the volume fraction and temperature coefficient of the resonant frequency of the ith phase, respectively. When x = 4, the ceramic exhibited a high ε_r value (42.5) and a τ_f of −59 ppm/°C due to the $Bi_4B_2O_9$ single phase. As x increased to 3, the $Q \times f$ increased to 4960 GHz. However, the relative permittivity of ceramic significantly decreased to 31. This was attributed to a higher $Q \times f$ but lower ε value of the $Bi_3B_5O_{12}$ ceramic [15].

The chemical compatibility of the $Bi_4B_{2+x}O_{9+3x/2}$ (x = 2.5) ceramic to Al and Ag was tested. Al and Ag powders were placed inside the samples and subsequently sintered at 585 °C to prevent Al powders from being exposed to air to form Al_2O_3. After being polished, the cross section of the ceramic sample was analysed using SEM and EDS. The SEM image shown in Fig. 8(a) indicates that no mutual diffusion phenomenon occurred and Ag, Al, and $Bi_4B_2O_9$ were spread in irrelevant areas. The Al and Ag phases were identified and no other phase was observed from the XRD patterns, as shown in Fig. 8(b). These results suggested that $Bi_4B_{2+x}O_{9+3x/2}$ (x = 2.5) ceramic did not react with Al or Ag at 585 °C, which means that the ceramic can be successfully applied in the ULTCC field.

4. Conclusion

$Bi_4B_{2+x}O_{9+3x/2}$ (x = 1.5, 2, 2.5, 3) microwave ceramics with high relative permittivity and ultra-low sintering temperature were investigated. When x = 2.5, the $Bi_4B_{2+x}O_{9+3x/2}$ ceramic displayed a single monoclinic $Bi_4B_2O_9$ phase, and the best microwave dielectric properties of ε_r = 42.5, $Q \times f$ = 3240 GHz, and τ_f = −59 ppm/°C appeared at 585 °C. Subsequently, decreasing or increasing the value of x caused the second phase to appear. As x decreased from 2.5 to 1.5, the emergence of Bi_2O_3 phase caused the ε_r and τ_f to decrease to 36.5 and –132 ppm/°C, respectively. When the value of x increased to 3, the ε_r value significantly decreased from 42.5 to 31.0 because of orthorhombic $Bi_3B_5O_{12}$. The $Bi_4B_{2+x}O_{9+3x/2}$ (x = 1.5, 2, 2.5, 3) ceramics could also be cofired with Al and Ag, implying that they can be new candidate materials for multilayer ULTCC or LTCC applications.

Declaration of competing interest

There are no conflicts to declare.

Acknowledgements

This work was supported by the Natural Science Foundation of China (Nos. 61761015 and 11664008) and the Natural Science Foundation of Guangxi (Nos. 2017GXNSFFA198011 and 2017GXNSFDA198027).

References

[1] L.H. Ouyang, W.Q. Wang, H.C. Fan, Z.Z. Weng, W.W. Wang, H. Xue, Sintering behavior and microwave performance of $CaSiO_3$ ceramics doped with $BaCu(B_2O_5)$ for LTCC applications, Ceram. Int. 45 (15) (2019) 18937–18942.
[2] W.J. Luo, L.X. Li, S.H. Yu, B.W. Zhang, J.L. Qiao, Raman, EPR and structural studies of novel $CuZrNb_2O_8$ ceramic for LTCC applications, Ceram. Int. 45 (12) (2019) 15314–15319.
[3] X.Q. Song, K. Du, Z.Y. Zou, Z.H. Chen, W.Z. Lu, S.H. Wang, W. Lei, Temperature-stable $BaAl_2Si_2O_8$-$Ba_5Si_8O_{21}$-based low-permittivity microwave dielectric ceramics

for LTCC applications, Ceram. Int. 43 (16) (2017) 14453–14456.
[4] Y.K. Yang, Y.Z. Wang, J.J. Zheng, N. Dai, H.T. Wu, B. Wu, Microwave dielectric properties of ultra-low loss $Li_2Mg_4Zr0.95(Mg_{1/3}Ta_{2/3})(0.05)O_7$ ceramics sintered at low temperature by LiF addition, J. Alloys Compd. 786 (25) (2019) 867–872.
[5] A. Pirvaram, E. Taheri-Nassaj, H. Taghipour-Armaki, W.Z. Lu, W. Lei, H.B. Bafrooei, Study on structure, microstructure and microwave dielectric characteristics of CaV_2O_6 and $(Ca_{0.95}M_{0.05})V_2O_6$ (M = Zn, Ba) ceramics, J. Am. Ceram. Soc. 102 (9) (2019) 5213–5222.
[6] L.X. Pang, D. Zhou, D.W. Wang, J.X. Zhao, W.G. Liu, Z.X. Yue, I.M. Reaney, Temperature stable $K_{-0.5}(Nd_{1-x}Bix)_{(0.5)}MoO_4$ microwave dielectrics ceramics with ultra-low sintering temperature, J. Am. Ceram. Soc. 101 (5) (2018) 1806–1810.
[7] X.Q. Song, W. Lei, Y.Y. Zhou, T. Chen, S.W. Ta, Z.X. Fu, W.Z. Lu, Ultra-low fired fluoride composite microwave dielectric ceramics and their application for $BaCuSi_2O_6$-based LTCC, J. Am. Ceram. Soc. 103 (2) (2020) 1140–1148.
[8] W. Wang, M.W. Zhang, L. Xin, S.T. Shen, J.W. Zhai, Effect of interface behavior on dielectric properties of ferroelectric-dielectric composite ceramics, J. Alloys Compd. 809 (15) (2019) 6–11.
[9] X.H. Wang, M.L. Mu, H. Jiang, W. Lei, W.Z. Lu, Investigation on structure and microwave dielectric properties of novel high dielectric constant $Ca_{(1-3x/2)}Ce_xTiO_3$ ceramics sintered in nitrogen atmosphere, J. Mater. Sci. Mater. Electron. 30 (2) (2019) 1591–1599.
[10] D. Zhou, L.X. Pang, D.W. Wang, I.M. Reaney, $BiVO_4$ based high k microwave dielectric materials: a review, J. Mater. Chem. C. 6 (35) (2018) 9290–9313.
[11] A.G. Belous, Microwave dielectrics with enhanced permittivity, J. Eur. Ceram. Soc. 26 (10–11) (2006) 1821–1826.
[12] M. Eberstein, W.A. Schiller, Development of high-permittivity glasses for microwave LTCC tapes, Glass Sci. Technol. 76 (1) (2003) 8–16.
[13] D. Zhou, C.A. Randall, H. Wang, L.X. Pang, X.S. Yao, Microwave dielectric ceramics in Li_2O–Bi_2O_3–MoO_3 system with ultra-low sintering temperatures, J. Am. Ceram. Soc. 93 (4) (2010) 1096–1100.
[14] D. Zhou, C.A. Randall, L.X. Pang, H. Wang, J. Guo, G.Q. Zhang, Y. Wu, K.T. Guo, L. Shui, X. Yao, Microwave dielectric properties of $(ABi)_{(1/2)}MoO_4$ (A = Li, Na, K, Rb, Ag) type ceramics with ultra-low firing temperatures, Mater. Chem. Phys. 129 (3) (2011) 688–692.
[15] X. Chen, W. Zhang, B. Zalinska, I. Sterianou, S. Bai, I.M. Reaney, Low sintering temperature microwave dielectric ceramics and composites Based on Bi_2O_3–B_2O_3, J. Am. Ceram. Soc. 95 (10) (2012) 3207–3213.
[16] K. Wang, T. Yin, H. Zhou, X. Liu, J. Deng, S. Li, C. Lu, X. Chen, Bismuth borate composite microwave ceramics synthesised by different ratios of H_3BO_3 for ULTCC technology, J. Eur. Ceram. Soc. 40 (2) (2020) 381–385.
[17] B.H. Toby, EXPGUI, a graphical user interface for GSAS, J. Appl. Crystallogr. 34 (34) (2001) 210–213.
[18] A.V. Egorysheva, V.I. Burkov, Y.F. Kargin, V.G. Plotnichenko, V.V. Koltashev, Vibrational spectra of crystals of bismuth borates, Crystallogr. Rep. 50 (1) (2005) 127–136.
[19] X.K. Lan, J. Li, Z.Y. Zou, G.F. Fan, W.Z. Lu, W. Lei, Lattice structure analysis and optimised microwave dielectric properties of $LiAl_{1-x}(Zn_{0.5}Si_{0.5})_xO_2$ solid solutions, J. Eur. Ceram. Soc. 39 (7) (2019) 2360–2364.
[20] H. Ghobadi, W.Z. Lu, W. Lei, K. Du, F. Wang, An evaluation of the impact of crystal symmetry on microwave dielectric properties of $Sr_{1-2x}Nd_{2x}Ti_{1-x}Mg_xO_3$ solid solution, Ceram. Int. 45 (15) (2019) 18529–18535.
[21] W. Liu, R. Zuo, A novel low-temperature firable $La_2Zr_3(MoO_4)_9$ microwave dielectric ceramic, J. Eur. Ceram. Soc. 38 (1) (2018) 339–342.
[22] S. Roberts, Polarizabilities of ions in perovskite-type crystals, Phys. Rev. 5 (81) (1951) 865–868.
[23] D. Zhou, L.X. Pang, H.D. Xie, J. Guo, B. He, Z.M. Qi, T. Shao, X. Yao, C.A. Randall, Crystal structure and microwave dielectric properties of an ultralow-temperature-fired $(AgBi)_{0.5}WO_4$ ceramic, Eur. J. Inorg. Chem. 2 (21) (2014) 296–301.
[24] R.D. Shannon, Dielectric polarizabilities of ions in oxides and fluorides, J. Appl. Phys. 1 (73) (1993) 348–366.
[25] X.Q. Song, K. Du, J. Li, X.K. Lan, W.Z. Lu, X.H. Wang, W. Lei, Low-fired fluoride microwave dielectric ceramics with low dielectric loss, Ceram. Int. 45 (1) (2019) 279–286.
[26] B. Ullah, W. Lei, X.H. Wang, G.F. Fan, X.C. Wang, W.Z. Lu, Dielectric and ferroelectric behavior of an incipient ferroelectric $Sr_{(1-3x/2)}Ce_xTiO_3$ novel solid solution, RSC Adv. 6 (94) (2016) 91679–91688.
[27] W. Lei, Z.Y. Zou, Z.H. Chen, B. Ullah, A. Zeb, X.K. Lan, W.Z. Lu, G.F. Fan, X.H. Wang, X.C. Wang, Controllable τ_f value of barium silicate microwave dielectric ceramics with different Ba/Si ratios, J. Am. Ceram. Soc. 101 (1) (2018) 25–30.